Solid State Science and Technology, Vol. 24, No 1(2016) 30-40
ISSN 0128-7389 | *http://journal.masshp.net*

INCORPORATION OF CARBON NANOTUBES IN In_2O_3 THIN FILMS FOR GREATER DSSC PERFORMANCE

Savisha Mahalingam[1], H Abdullah[1],
Sahabudin Shaari[2], and Andanastuti Muchtar[3]

[1]*Department of Electrical, Electronic & System,*
Faculty of Engineering and Built Environment,
Universiti Kebangsaan Malaysia, 43600 Bangi, Selangor, Malaysia

[2]*Institute of Microengineering and Nanoelectronics (IMEN), Universiti Kebangsaan Malaysia, 43600 Bangi, Selangor, Malaysia*

[3]*Department of Mechanical and Materials Engineering,*
Faculty of Engineering and Built Environment,
Universiti Kebangsaan Malaysia, 43600 Bangi, Selangor, Malaysia.

Corresponding author: huda@eng.ukm.my

ABSTRACT

In_2O_3 is a wide band gap material which has a potential application in dye-sensitized solar cells (DSSCs). The objective of this research is to enhance the photovoltaic conversion efficiency in In_2O_3 thin films by incorporating MWCNTs and SWCNTs in the nanocomposite. In_2O_3 incorporating CNTs annealed at 450 °C was prepared by using spin-coating method for DSSCs. The structural and morphological characteristics of In_2O_3 thin films were studied via XRD patterns and atomic force microscopy (AFM). The In_2O_3-SWCNTs based DSSCs exhibited better photovoltaic performance than In_2O_3-based DSSCs with a conversion efficiency of 1.11 %. The electrochemical impedance spectroscopy (EIS) unit investigated the charge transfer process inside the DSSCs. A longer electron lifetime with a high recombination rate was found in In_2O_3-SWCNTs. These two factors speeds up the electron transport in the cell and enhanced the PCE of the DSSCs.

Keywords: In_2O_3-MWCNTs; In_2O_3-SWCNTs; morphology; electrical; DSSCs;

INTRODUCTION

Dye-sensitized solar cells (DSSCs) were first introduced by O'Regan and Grätzel in 1991 [1]. DSSCs were more favourable compared to other types of solar cells due to their low cost production, fabrication ease, environmental friendly and flexibility. Besides that, the reasonably high performance of DSSCs makes them a desirable type of solar cell by the consumers. To date, the TiO_2-based DSSCs have achieved the highest power conversion efficiency (PCE) of ~15 % as reported by Burschka *et al.* [2].

However, alternative metal oxides such as ZnO [3], In_2O_3 [4] and SnO_2 [5] have higher electron mobility than TiO_2 that speeds up the electron transport and improves the PCE of the cell.

In_2O_3 is a wide band gap material with a direct band gap and indirect band gap of 3.6 eV and 2.6 eV, respectively [6]. In_2O_3 is rarely used as photoanode material in DSSCs as it exhibits low PCE compared to TiO_2 materials even if it has high electron mobility as mentioned above. Recently, carbon nanotubes (CNTs) have been used to combine with the photoanode materials such as TiO_2-CNT, ZnO-CNT and SnO_2-CNT to increase the PCE of DSSCs [5, 7, 8]. Introduction of CNTs in the metal oxides improves the electrical conductivity by providing fast electron transfer kinetics which was observed through electrochemical impedance spectroscopy (EIS) unit [9]. Moreover, in terms of morphology incorporation of CNTs induce pores that able to improve light harvesting efficiency in the electrode making an easy pathway for dye-adsorption.

In this paper, we report the DSSC performance of In_2O_3 and incorporation CNTs with In_2O_3 as photoanode material. There are two types of CNTs which are multi-walled carbon nanotubes (MWCNTs) and single-walled carbon nanotubes (SWCNTs). These two CNTs are used to incorporate with In_2O_3 nanoparticles. The main aim of this report is to improve the low performance of In_2O_3-based DSSCs by introducing MWCNTs and SWCNTs. The structure, morphology and electrical properties of In_2O_3-CNTs were studied carefully.

EXPERIMENTAL DETAILS

Preparation of Thin Films.
Sol-gel method was used to prepare In_2O_3 thin films via spin-coating technique as shown in Figure 1. All the chemical reagents were purchased from Sigma-Aldrich (USA). 0.1 M of Indium chloride ($InCl_3$) was dissolved in 50 ml of 2-methoxyethanol to form a stable transparent aqueous solution. The mixture was stirred on a hot plate for 24 h at 60 °C. After the cooling process, the mixture was spin-coated with five layers on a Fluorine-doped tin oxide (FTO) coated glass substrate by using a spin coater (Model WS-400BX-6NPP/LITE). The spin-coated In_2O_3 films were annealed at 450 °C for 30 min in an electric furnace. The same procedure took place to prepare In_2O_3-CNTs except in the first step 0.1 M of $InCl_3$ powder and 0.1 % of CNTs were mixed together and dissolved in 50 ml of 2-methoxyethanol.

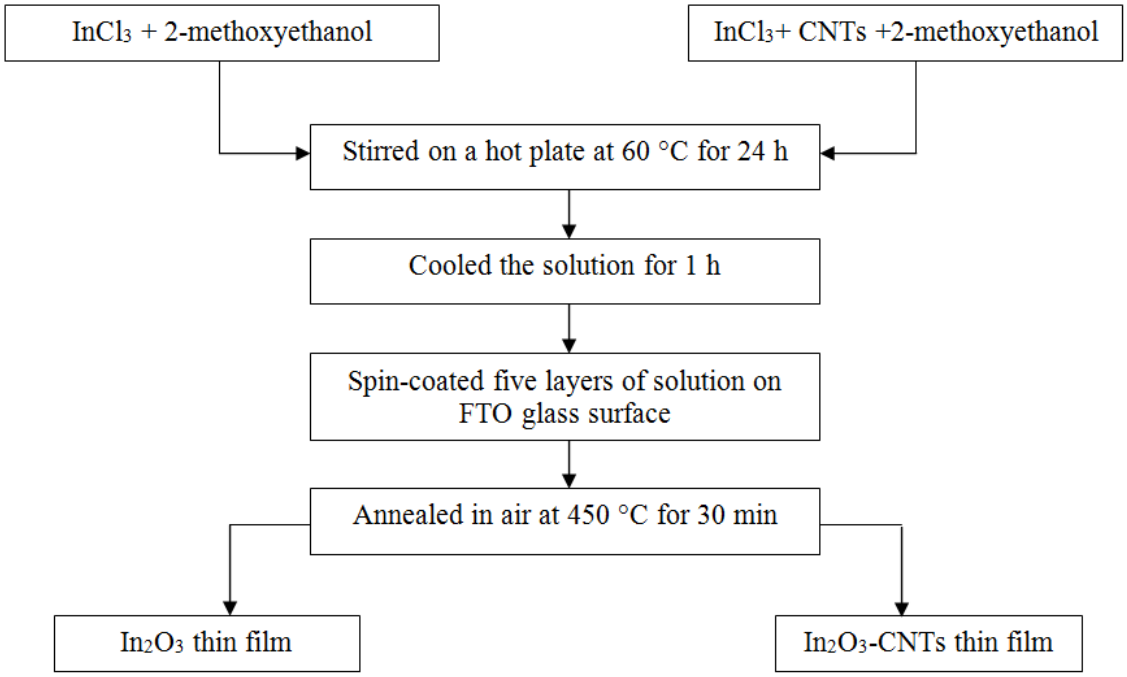

Figure 1: Flow chart of In_2O_3 and In_2O_3-CNTs thin films preparation process

Fabrication of DSSCs.
The annealed thin films were immersed in ethanolic N719 dye (0.5 mM) for 24 h in a glass petri dish. At the same time, the counter electrode (CE) was prepared by pasting platinum paste on a clean FTO glass substrate via screen printing technique. The CE is then annealed in air at 400 °C for 1 h. The DSSCs were fabricated by sandwiching the immersed photonode thin film and CE together. The DSSCs were assembled by using a parafilm layer and two binder clips with active area of 1 cm^2. Finally, the electrolyte (Idolyte MPN 100 Solaronix SA) was injected into the cell.

Characterization of DSSCs.
The structure and morphology of the photoanode thin films were characterized by X-ray diffractometer (XRD), atomic force microscopy (AFM) and field-emission scanning electron microscope (FESEM). The photovoltaic performance of the photoanode thin films was analyzed through photocurrent density-voltage (*J-V*) curve measurement. The electron transport properties were determined by EIS unit (GAMRY Series G300 Potentiostat).

RESULTS AND DISCUSSIONS

The structure of the thin films was confirmed through the XRD patterns. Figure 2 (a), (b) and (c) shows the XRD patterns of In_2O_3, In_2O_3-SWCNTs and In_2O_3-MWCNTs, respectively. The phase structure of In_2O_3 was confirmed as body-centered cubic with lattice constant, a of 10.117 Å (JCPDS no. 01-071-2194. From Figure 2, crystallinity of

the thin films were improved when CNTs were incorporated with In_2O_3 (Figure 2 (b) and (c)). However, when comparing the both CNTs, SWCNTs incorporated with In_2O_3 showed higher crystallinity than MWCNTs. The XRD patterns of In_2O_3 were attributed at 2θ = 26°, 30.575° and 35.475°, 37.70° and 51.043°, corresponding to the (*h k l*) miller indices of (211), (222), (400) and (440) planes. Orientation at (222) plane was considered as the preferred orientation [4].

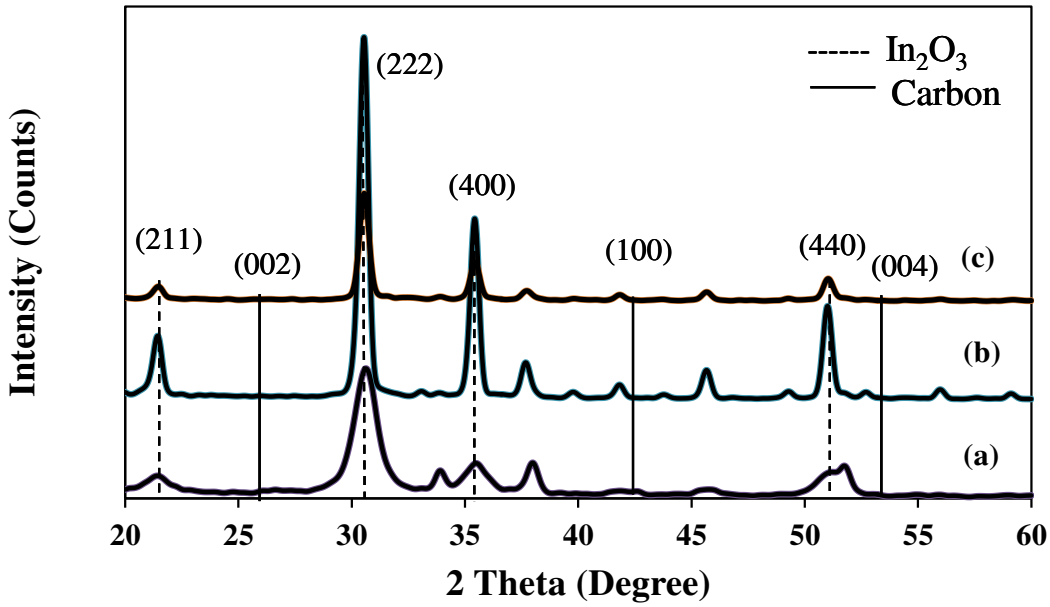

Figure 2: XRD spectra of (a) In_2O_3, (b) In_2O_3-SWCNTs and (c) In_2O_3-MWCNTs

Meanwhile, the carbon (C70) patterns were reflected at 2θ = 26.2°, 43.4° and 54.6°, reflecting to (002), (100) and (004) planes. The peak intensities of carbon were very small due to the low concentration of only 0.1 % of CNTs were added in the composite. The result confirmed that the In_2O_3-CNTs possess a carbonic character in their pore walls. Furthermore, the crystallite size (*D*) was calculated by using Debye-Scherrer's formula [11]:

$$D = \frac{k\lambda}{\beta \cos\theta} \qquad (1)$$

where, k is the Scherrer's constant with 0.94 and β is the full width at half maximum (FWHM) of the Bragg peak. Table 1 shows the crystallite sizes of the In_2O_3 nanoparticles. The crystallite sizes of the In_2O_3 nanoparticles decreased when CNTs were incorporated in the nanocomposite. In addition, Abdullah *et al.* mentioned that incorporation of CNTs decreases the *D* [10].

Table 1: Crystallite sizes and surface roughness of the thin films

Samples	**hkl**	**2θ (°)**	***D* (nm)**	**R_a (nm)**
In_2O_3	(222)	30.59	19.21	0.35
In_2O_3-MWCNTs	(222)	30.54	16.52	3.54
In_2O_3-SWCNTs	(222)	30.51	15.32	6.62

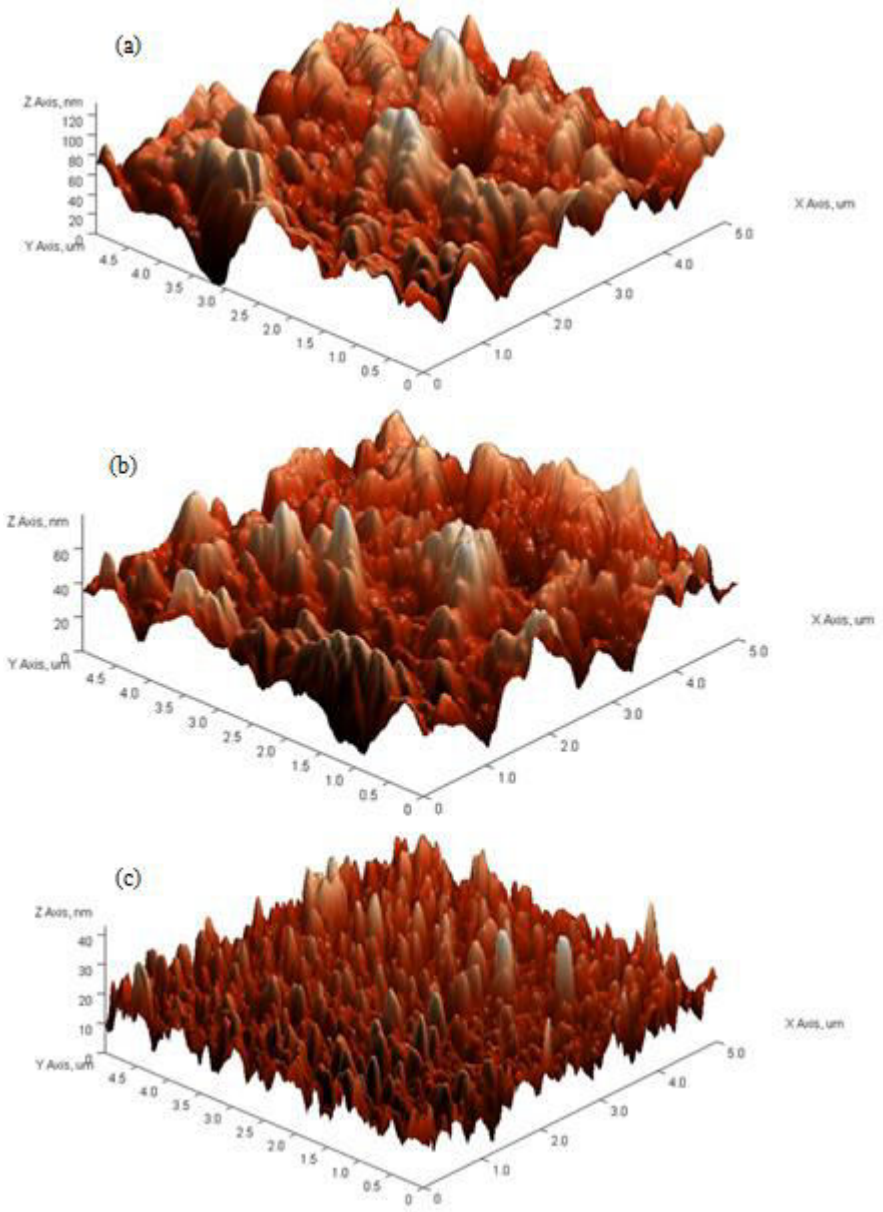

Figure 3: AFM images of (a) In_2O_3, (b) In_2O_3-SWCNTs and (c) In_2O_3-MWCNTs

The AFM and FESEM analysis were done to analyze the morphological characterization of the photoanodes. Figure 2 (a), (b) and (c) shows the AFM images of In_2O_3, In_2O_3-MWCNTs and In_2O_3-SWCNTs, respectively. The surface roughness of the thin films is listed in Table 1. Figure 2 (b) and (c) shows more columnar grain growth which signifies the thin films consist of rougher surface structure. The AFM result denotes that incorporation of CNTs provide rougher surface which improves the short circuit current density (J_{sc}) of the cell by increasing the light adsorption [12]. Additionally, Uk Lee *et al.* stated that a photoanode with rough surface structure bounces the incident light that hits the surface and reflects the light indirectly back on the surface of the thin film [13]. Therefore, more incident light is able to be captured by the dye molecules that are on the surface of the films. In_2O_3-SWCNTs have rougher surface roughness than In_2O_3-MWCNTs as seen from Table 1.

The photovoltaic performance of the DSSCs was measured with light intensity of 100 mW/cm2 under Am 1.5. Figure 4 (a), (b) and (c) shows the *J-V* characteristics of In_2O_3, In_2O_3-SWCNTs and In_2O_3-MWCNTs, respectively. The conversion of solar energy to electricity which is the PCE of the DSSCs is expressed in percentage. The photovoltaic performances of In_2O_3, In_2O_3-SWCNTs and In_2O_3-MWCNTs are listed in Table 2. The photovoltaic parameters include J_{sc}, open-circuit voltage, V_{oc}, fill factor, *FF* and PCE.

From Table 2, In_2O_3-based DSSCs generated low PCE of 0.55 % with low J_{sc}, V_{oc} and *FF* of 3.6 mA/cm^2, 0.34 V and 0.4, respectively. The obtained J_{sc} and V_{oc} increased as CNTs were added to In_2O_3 solution. We monitored that, In_2O_3-SWCNTs exhibited higher J_{sc} of 5.6 mA/cm^2 compared to In_2O_3-MWCNTs. In_2O_3-SWCNTs attained higher J_{sc} due to the higher roughness of the thin films by allowing more dye molecules to be adsorbed on the surface of the films. In addition, previous literatures stated that high roughness factor on the surface of the thin films increased dye adsorption in the photoanode layer [9, 14, 15]. However, the V_{oc} and *FF* of In_2O_3-MWCNTs and In_2O_3-SWCNTs did not vary much. This is because, V_{oc} depends on the nanocomposite conduction band egde and electrolyte which is more or less similar for both samples [16]. Thus, a good interaction between In_2O_3 and SWCNTs happened in the photoanode layer. In conjunction to that, Lee *et al.* reported that good interaction of metal oxide with CNTs provide longer electron lifetime and inhibits electron recombination in DSSCs [17]. Therefore, the EIS unit was used to determine the electron transport parameters that influenced the overall PCE and J_{sc}.

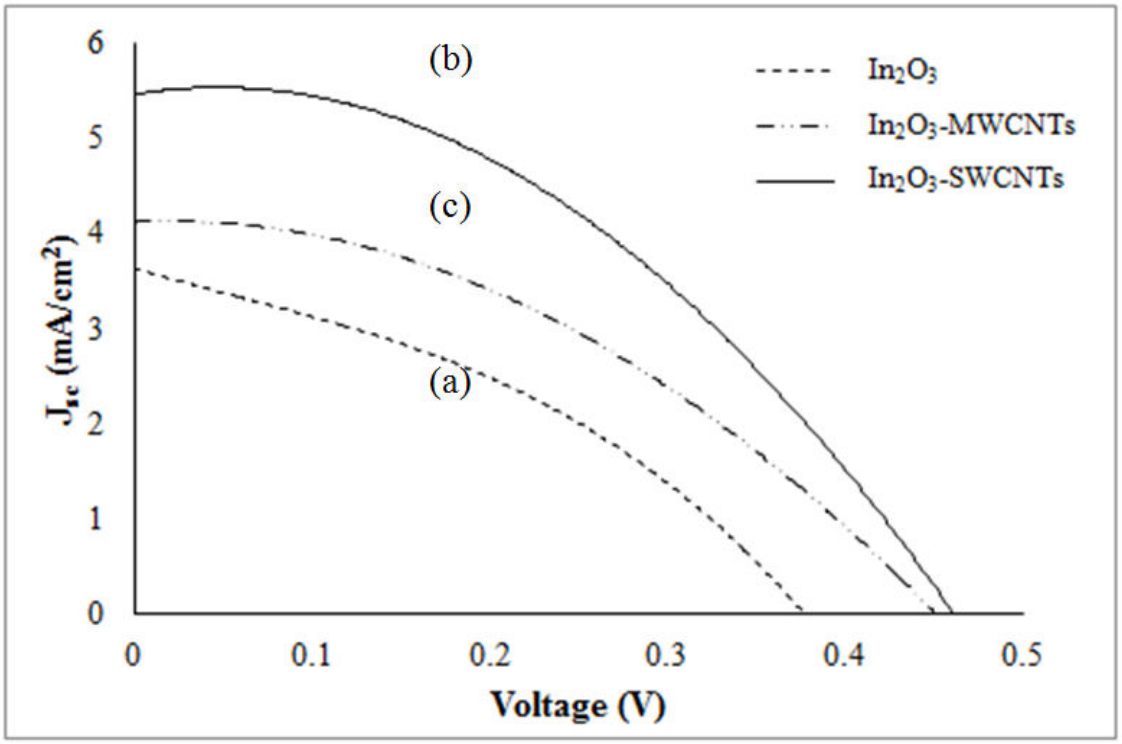

Figure 4: *J-V* characteristics of (a) In_2O_3, (b) In_2O_3-SWCNTs and (c) In_2O_3-MWCNTs

Table 2: Photovoltaic performances of ZnO-MWCNTs based DSSC

Samples	J_{sc} **(mA/cm^2)**	V_{oc} **(V)**	***FF***	**PCE (%)**
In_2O_3	3.6	0.38	0.4	0.55
In_2O_3-MWCNTs	4.32	0.45	0.43	0.84
In_2O_3-SWCNTs	5.60	0.46	0.43	1.11

EIS analysis was done in order to analyse the reasons of low performance in In_2O_3-based DSSCs and higher performance in In_2O_3-SWCNTs-based DSSCs. EIS analysis was conducted under the illumination of 100 mW/cm^2. Figure 5 shows the Nyquist spectra of (a) In_2O_3, (b) In_2O_3-SWCNTs and (c) In_2O_3-MWCNTs. The Nyquist plots were then fitted by an equivalent circuit model proposed by Mahalingam *et al.* [4]. The circuit is based on the physical structure of the DSSCs.

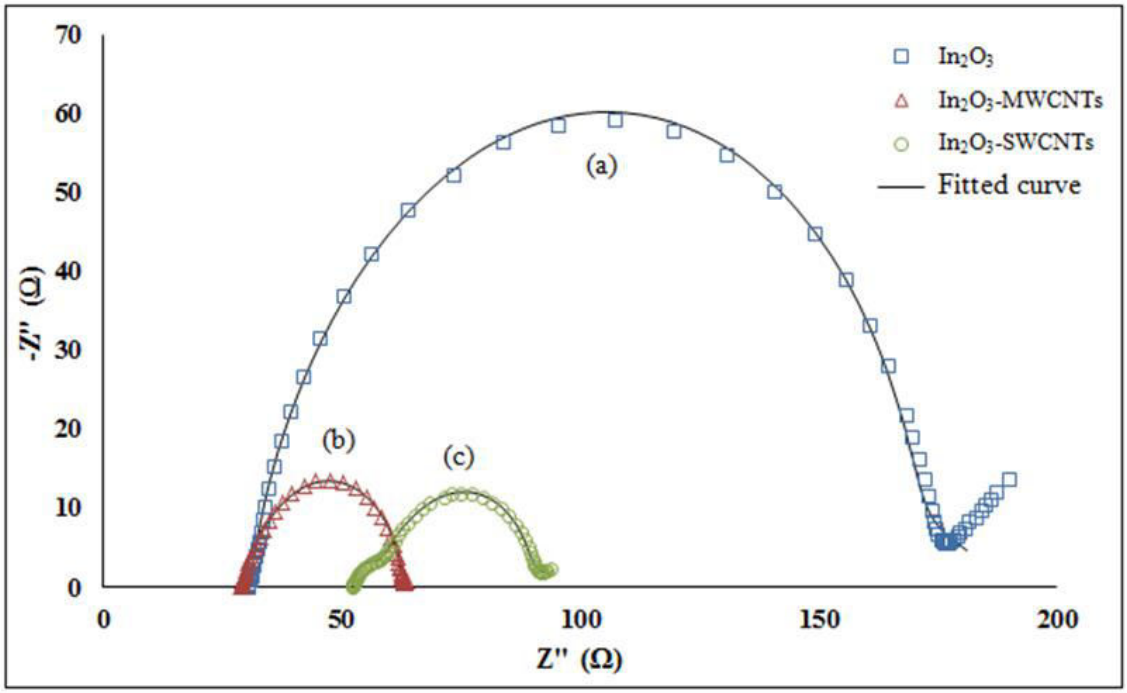

Figure 5: EIS plots of (a) In_2O_3, (b) In_2O_3-MWCNTs and (c) In_2O_3-SWCNTs

Different frequencies in each impedance spectra represent the photoanode, electrolyte and counter electrode part. The high, medium and low frequency regions represent the counter electrode, photoanode and electrolyte, respectively. The electron transport parameters with DSSCs performance is listed in Table 3 where, R_s is the sheet resistance, R_t is the electron transport resistance and R_{ct} is the charge-transfer resistance [18,19,20-24].

Table 3: Electron transport parameters of In_2O_3, In_2O_3-SWCNTs and In_2O_3-MWCNTs based DSSCs

DSSC	f_{max} **(Hz)**	ω_{max} **(Hz)**	R_s **(Ω)**	R_{ct} **(Ω)**	R_t **(Ω)**	τ_{eff} **(ms)**	k_{eff} **(s^{-1})**	**PCE (%)**
In_2O_3	476	2989	29.09	35.51	1.54×10^{-3}	0.335	2985	0.55
In_2O_3-MWCNTs	378	2374	28.97	155.7	2.615	0.421	2375	0.84
In_2O_3-SWCNTs	37.5	236	27.14	676.1	2.682	4.24	236	1.11

Furthermore, the maximum frequency, f_{max} of the Nyquist plot is the peak frequency at the photoanode region. We can then measure the ω_{max} since, $\omega_{max}=2\pi f_{max}$. The electron lifetime, τ_{eff}, effective electron diffusion coefficient, D_{eff} and electron recombination rate, k_{eff} can also be calculated by following equations [18,19]:

$$\tau_{eff} = \frac{1}{(2\pi f_{\max})} \quad (2)$$

$$k_{eff} = \frac{1}{\tau_{eff}} \quad (3)$$

From the fitted curves of impedance spectra (Figure 5), In_2O_3-SWCNTs achieved the highest τ_{eff} of 4.24 ms. In contrast, In_2O_3-based DSSCs achieved the lowest τ_{eff} of 0.335 ms. Consequently, short electron lifetime decreases the J_{sc} of In_2O_3-based DSSCs to 3.6 mA/cm^2. In addition, doping of SWCNTs decreased the R_s to 27.14 Ω. Hara *et al.* mentioned that, decrease of R_s can improve V_{oc} and *FF* [25]. In conjunction to that, addition of CNTs in In_2O_3 solution improved V_{oc} and *FF* in the cell where value of R_s decreased when CNTs were added to In_2O_3. Besides that, the spectrum of In_2O_3 showed no arc at the high frequency part due to Warburg diffusion of the redox couple of electrolyte. Thus, the low V_{oc} and *FF* obtained in In_2O_3 based DSSCs were also due to the missing arc. Moreover, In_2O_3 based DSSCs showed the lowest value of R_{ct} with 35.51 Ω. Smaller R_{ct} speeds up the electron recombination rate, k_{eff} to 2985 s^{-1}. This event indicated that, more injected electrons were recombined with the electron acceptors that slowed down the electron transport process thus, degraded the PCE of In_2O_3 based DSSCs.

CONCLUSION

In summary, In_2O_3 and In_2O_3-CNTs based DSSCs were successfully synthesized and fabricated by spin coating technique. MWCNTs and SWCNTs were added to In_2O_3 solution in order to improve the low performance of In_2O_3-based DSSCs. The XRD confirmed the In_2O_3 cubic structure and the crystallite size decreased as the CNTs were incorporated with In_2O_3. The AFM images also proved addition of CNTs increased the surface roughness of the thin films allowing more dye molecules to be adsorbed on the thin films thus increased the J_{sc}. However, In_2O_3-SWCNTs possessed smaller crystallite size and rougher surface roughness than In_2O_3-MWCNTs. I conjunction to those factors, In_2O_3-SWCNTs exhibited the highest PCE of 1.11 % with J_{sc}, V_{oc} and *FF* of 5.60 mA/cm^2, 0.46 V and 0.43, respectively. Moreover, In_2O_3-SWCNTs showed the highest electron lifetime and lowest electron recombination rate of 4.24 ms and 236 s^{-1}, respectively. Longer τ_{eff} in In_2O_3-SWCNTs caused the J_{sc} to increase up to 5.6 mA/cm^2. In addition, the highest R_{ct} in In_2O_3-SWCNTs slowed down the electron recombination rate and speeds up the electron transport in the cell. Therefore, addition of CNTs in In_2O_3 solution enhanced the PCE of the DSSCs. However, in comparison to the types of CNTs, SWCNTs exhibited higher performance in In_2O_3-based DSSCs.

ACKNOWLEDGEMENTS

This work was funded by Fundamental Research Grant Scheme (FRGS/2/2013/TK06/UKM/02/3), Photonic Technology Laboratory (IMEN) and

Department of Electrical, Electronic & Systems Engineering, Universiti Kebangsaan Malaysia, Bangi, Selangor, Malaysia.

REFERENCES

[1]. B. O'regan, M. Grätzel, Nature **353** (1991) 737-740
[2]. J. Burschka, N. Pellet, S.J. Moon, R.H. Baker, P. Gao, M.K. Nazeeruddin, M. Grätzel, *Nature* **499** 316-319 (2013)
[3]. H. Abdullah, N.A. Atiqah, A. Omar, I. Asshaari, S. Mahalingam, Z. Razali, S. Shaari, J.S. Mandeep, H. Misran, *Journal of Materials Science: Materials in Electronics* **26** 2263-2270 (2015)
[4]. S. Mahalingam, H.Abdullah, S. Shaari, A. Muchtar, I. Asshari, Structural, morphological and electron transport studies of annealing dependent In_2O_3 dye-sensitized solar cell, *The scientific World Journal* **2015**, Article ID 403848, (2015).
[5]. S. Mahalingam, H. Abdullah, A. Omar, N.A.M. Nawi, S. Shaari, A. Muchtar, I. Asshari, *Advanced Materials Research,* **1107** 649-654 (2015)
[6]. A. Raza, O.P. Agnihotri, B.K. Gupta, *Journal of Physics D: Applied Physics* **10** 1871 (1977)
[7]. M.Z. Razali, H. Abdullah, S. Shaari, M.R. Taha, A. Omar, M.A. Yarmo, *Journal of Nano Research* **28** 151-162 (2014)
[8]. A. Omar, H. Abdullah, S. Shaari, M.R. Taha, *Journal of Materials Research* **28** 1753-1760 (2013)
[9]. A. Omar, H. Abdullah, M.A. Yarmo, S. Shaari, M.R. Taha, *J. Phys. D Appl. Phys*. **46** 165503 (2013)
[10]. H. Abdullah, M.Z. Razali, S. Shaari, M.R. Taha, *Electron. Mater. Lett.* **10** 611-619 (2014)
[11]. S. Bucak, D. Rende, Colloid and surface chemistry: A laboratory guide for exploration of the nano World, CRCPress, New York, NY, USA, 2014.
[12]. N.P. Ariyanto, H. Abdullah, N.S.A. Ghani, *Materials Research Innovations,* **13** 157-160 (2009)
[13]. S. Uk Lee,W. Seok Choi, B. Hong, *Solar Energy Materials and Solar Cells,* **94** 680-685 (2010)
[14]. Y. Zhang, M.K. Ram, E.K. Stefanakos, D.Y. Goswami, *J. Nanomat.* **2012** 1-22 (2012)
[15]. N. Karst, G. Rey, B. Doisneau, H. Roussel, R. Deshayes,V. Consonni, C. Ternon, D. Bellet, *Mat. Sc.i & Eng. B* **176** 653–659 (2011)
[16]. G.S.Y. Schlichthörl, S.Y. Huang, J. Sprague, A.J. Frank, *Journal of Physical Chemistry B* **101** 8141-8155 (1997)
[17]. K.M. Lee, C.H. Hu, H.W. Chen, K.C. Ho, *Solar Energy Materials and Solar Cells* **92** 1628-1633 (2008)
[18]. M. Adachi, M. Sakamoto, J. Jiu, Y. Ogata, S. Isoda, *J. Phys. Chem. B* **110** 13872-13880 (2006)
[19]. W.H. Chiu, C.H. Lee, H.M. Cheng, H.F. Lin, S.C. Liao, J.M. Wu, W.F. Hsieh, *Energy & Environ. Sci.* **2** 694-698 (2009)

[20]. J. Bisquert, *J. Phys. Chem. B* **2** 325-333 (2002)
[21]. F. Fabregat-Santiago, J. Bisquert, G. Garcia-Belmonte, G. Boschloo, A. Hagfeldt, *Sol. Energy Mat. & Sol. Cells* **87** 117-131 (2005)
[22]. Q. Wang, S. Ito, M. Grätzel, F. Fabregat-Santiago, I. Mora-Seró, J. Bisquert, T. Bessho, H. Imai, *J. Phys. Chem. B* **110** 25210-25221 (2006)
[23]. F. Fabregat-Santiago, J. Bisquert, E. Palomares, L. Otero, D. Kuang, S.M. Zakeeruddin, M. Grätzel, *J. Phys. Chem. C* **111** 6550-6560 (2007)
[24]. A.B.F. Martinson, M.S. Góes, F. Fabregat-Santiago, J. Bisquert, M.J. Pellin, J.T. Hupp, *J. Phys. Chem.* **113** 4015-4021 (2009)
[25]. K. Hara, T. Horoguchi, T. Kinoshita, K. Sayama, H. Sugihara, H. Arakawa, *Solar Energy Materials and solar cells* **64** 115-134 (2000)